Thermomechanical Analysis of Solder Joints Under Thermal and Vibrational Loading

Cemal Basaran
Assoc. Prof., and Director,
UB Electronic Packaging Laboratory,
University at Buffalo SUNY,
Buffalo, NY 14260
e-mail: cjb@eng.buffalo.edu

Rumpa Chandaroy
Staff Consultant,
Altair Engineering Inc.,
Detroit, MI 48071

Due to the coefficient of thermal expansion (CTE) mismatch between the bonded layers, the solder joint experiences cycling shear strain, which leads to short cycle fatigue. When semiconductor devices are used in a vibrating environment, additional strains shorten the fatigue life of a solder joint. Reliability of these joints in new packages is determined by laboratory tests. In order to use the FEM to replace these expensive reliability tests a unified constitutive model for Pb40/Sn60 solder joints has been developed and implemented in a thermo-viscoplastic-dynamic finite element procedure. The model incorporates thermal-elastic-viscoplastic and damage capabilities in a unified manner. The constitutive model has been verified extensively against laboratory test data. The finite element procedure was used for coupled thermo-viscoplastic-dynamic analyses for fatigue life predictions. The results indicate that using Miner's rule to calculate accumulative damage by means of two separate analyses, namely dynamic and thermo-mechanical, significantly underestimates the accumulative total damage. It is also shown that a simultaneous application of thermal and dynamic loads significantly shortens the fatigue life of the solder joint. In the microelectronic packaging industry it is common practice to ignore the contribution of vibrations to short cycle fatigue life predictions. The results of this study indicate that damage induced in the solder joints by vibrations have to be included in fatigue life predictions to accurately estimate their reliability.
[DOI: 10.1115/1.1400752]

Introduction

When semiconductor devices are used in a vibrating environment, dynamic strains contribute to the failure mechanism and can sometimes become the cause for dominant failure. Presently in the microelectronics industry, all vibration-induced stresses on solder joints are considered to be elastic. It is assumed that there is no contribution to the low cycle fatigue life from vibrations, Barker et al. [1]. In this paper it is shown that vibration effects cannot be classified categorically as elastic only and ignored in low cycle fatigue studies. It is also shown that at elevated temperatures, irreversible strains due to vibrations are greatly amplified. In this study it was observed that even the dynamic loads that are too small to induce irreversible deformations, could induce significant damage when coupled with thermal cycling.

A unified damage mechanics based constitutive model has been developed and then implemented in a nonlinear finite element analysis procedure for fatigue life analysis under coupled dynamic and thermal loads. The purpose of the study has been to observe the contribution of thermal and vibration induced strains to the fatigue life of solder joints. The fatigue life of the solder joint was determined by Miner's rule and also by coupled finite element analyses. For Miner's rule the damage due to each load type acting individually was determined and then superposed to assess the overall fatigue life of the joint. It should be pointed out that Miner's rule is commonly used in the industry, Barker et al. [1], Steinberg [2]. In coupled analyses both vibrations and thermal cycling were applied simultaneously and the fatigue life was directly computed by the finite element code.

Material Model

The constitutive model proposed in this paper is based on the Disturbed State Concept (DSC). The DSC has been used extensively for modeling geomaterials, concrete, metals and alloys, Desai [3], Desai and Toth [4], Desai et al. [5], Basaran et al. [6,7], Basaran and Chandaroy [8,9,10,11]. The DSC is a material modeling approach, which treats the continuum as an inhomogeneous mixture rather than as a homogeneous medium. According to the DSC, the continuum is composed of intact and fully adjusted parts. The intact part represents the virgin material reference state. The fully adjusted part represents the material that is in the residual asymptotic reference state. The fully adjusted part can be assigned different reference states for different materials. In this study it is assumed that in the fully adjusted state, the material cannot carry any shear stress but can carry hydrostatic compressive stresses only. We will refer to this particular definition of the fully adjusted state as the damaged state.

The incremental stress-strain relation in the DSC can be given by Desai [2], Basaran et al. [6]

$$d\sigma_{ij}^{a} = C_{ijkl}^{DSC} d\varepsilon_{kl}^{i} \tag{1}$$

where $d\sigma_{ij}^{a}$ is the incremental average stress tensor, $d\varepsilon_{kl}^{i}$ is the incremental strain tensor for the intact part, and the DSC tangential constitutive tensor is given by,

$$C_{ijkl}^{DSC} = [(1-D)^{i}C_{ijkl}^{evp\theta} + D(1+\alpha)^{c}C_{ijkl}^{evp\theta} + (\sigma_{ij}^{c} - \sigma_{ij}^{i})R_{kl}] \tag{2}$$

where ${}^{i}C_{ijkl}$ and ${}^{c}C_{ijkl}$ are the tangential constitutive tensors for the intact and damaged parts respectively, σ_{ij}^{c} and σ_{ij}^{i} are the total stress tensors for the damaged and intact parts, respectively, D is the accumulative damage, α is the empirical relative strain coefficient, and R_{kl} is the material moment tensor.

In this proposed model a damage criterion based on the second law of thermodynamics and statistical continuum mechanics is used. The damage model utilizes entropy, which is a measure of disorder in the system as a damage metric, Basaran and Yan [10]. Boltzmann [11], using statistical mechanics, gave a precise meaning to disorder and established the connection between disorder and entropy by the following equation,

Contributed by the Electronic and Photonic Packaging Division for publication in the JOURNAL OF ELECTRONIC PACKAGING. Manuscript received at ASME Headquarters March 15, 2001. Associate Editor: Yi-Hain Pao.

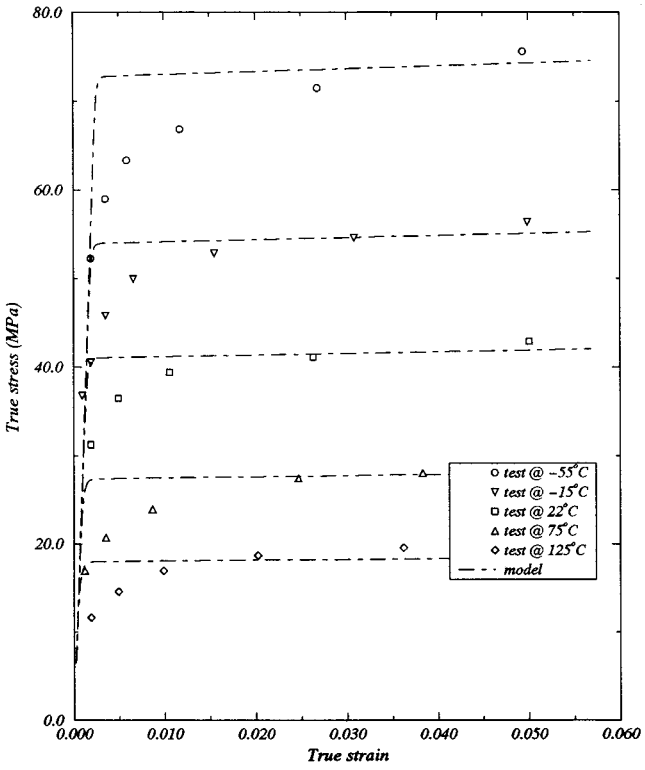

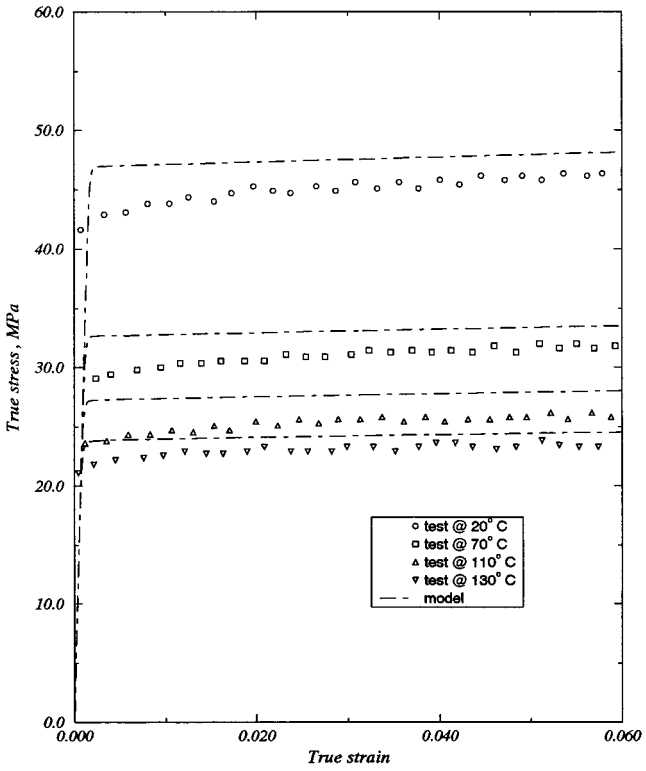

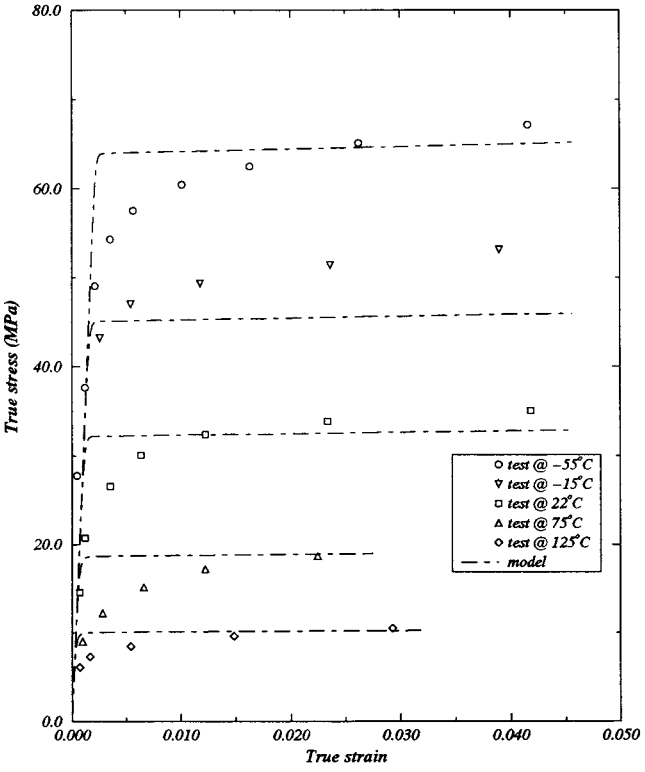

Fig. 1 (*a*) Comparison of stress versus strain results at different temperatures for strain rate of 1.67×10^{-3} (*b*) Comparison of stress versus strain results at different temperatures for strain rate of 1.67×10^{-4}

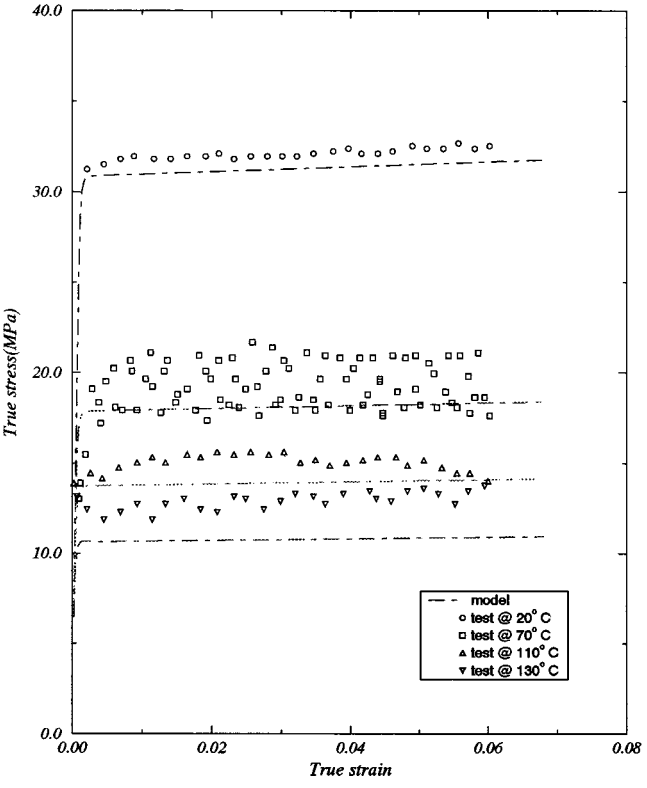

Fig. 2 (*a*) Comparison of stress versus strain results at different temperatures for strain rate of 1.0×10^{-2} (*b*) Comparison of stress versus strain results at different temperatures for strain rate of 1.0×10^{-4}

$$s = k \ln w \tag{3}$$

where s is the entropy, k is Boltzmann's constant and w is the disorder parameter, which is the probability that the system will exist in the state it is in relative to all the possible states, it could be in. ''This equation connects a thermodynamic and macroscopic quantity, the entropy, with a statistical microscopic quantity, the probability.'' Halliday and Resnick [12]

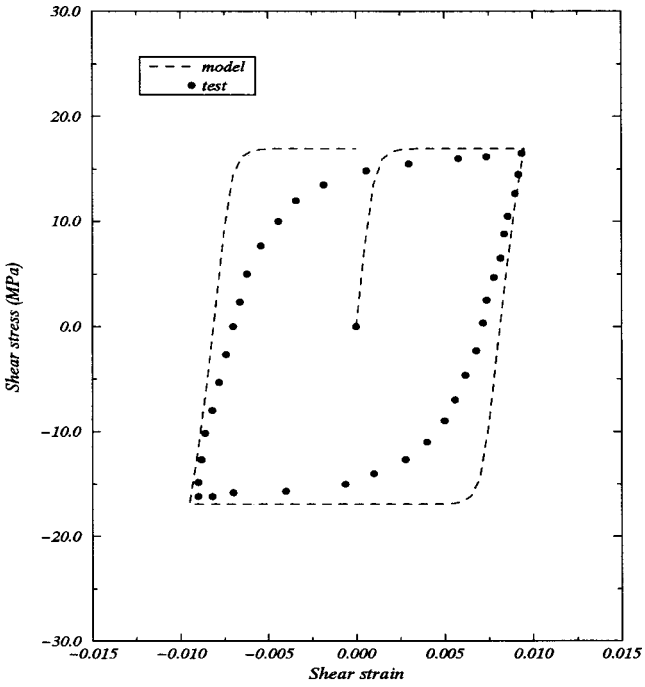

Fig. 3 Comparison of cyclic shear stress versus strain results at 25°C

The entropy in the context of the Helmholtz free energy function is given by,

$$\phi = e - \theta s \tag{4}$$

where ϕ is the Helmholtz free energy, e is the internal energy, θ is the absolute temperature and s is the entropy.

If we select an initial reference state of the material as state "o," then change in the disorder at any arbitrary time with respect to the initial reference state can be given by,

$$\Delta W = W_0 - W = e^{e_0 - \phi_0 / N_0 k \theta_0 / \bar{m}_s} - e^{e - \phi / N_0 k \theta / \bar{m}_s} \tag{5}$$

Using the definitions given in Eqs. (3) and (4) and also using the fundamental thermodynamic relations yields the following damage evolution function,

$$D = 1 - e^{-\Delta e - \Delta \phi / N_0 k \theta / \bar{m}_s} \tag{6}$$

where

$$\Delta e - \Delta \phi = \frac{1}{\rho}\left(\int_{\varepsilon_0}^{\varepsilon} \sigma_{ij} d\varepsilon_{ij}^{in} \right) - \frac{1}{\rho} \int_{t_0}^{t} \frac{\partial q_i}{\partial x_i} dt + \int_{t_0}^{t} \dot{\gamma} dt \tag{7}$$

where σ_{ij} is the total stress tensor, $d\varepsilon_{ij}^{in}$ is the incremental inelastic strain tensor, ρ is the unit mass density, q_i is the heat flux vector, $\dot{\gamma}$ is the distributed internal heat production rate per unit mass and dt is the time increment.

Thermo-Elasto-Viscoplasticity

In service Pb/Sn solder joints operate at high homologous temperature ($0.65\,T_m$), which is defined by T_{use}(Kelvin)/T_{melt}(Kelvin). Therefore, the contribution of creep to the fatigue damage becomes very significant. As a result, using a viscoplastic model for the characterization of the thermo-mechanical behavior of the Pb/Sn solder alloy is essential. Assuming small strains, the total strain increment tensor for a thermo elasto-viscoplastic problem can be separated into three parts:

$$d\varepsilon_{ij} = d\varepsilon_{ij}^{\theta} + d\varepsilon_{ij}^{e} + d\varepsilon_{ij}^{vp} \tag{8}$$

where $d\varepsilon_{ij}^{\theta}$, $d\varepsilon_{ij}^{e}$, and $d\varepsilon_{ij}^{vp}$ are the incremental thermal, elastic and viscoplastic strain tensors, respectively. The thermal strain increment is defined by,

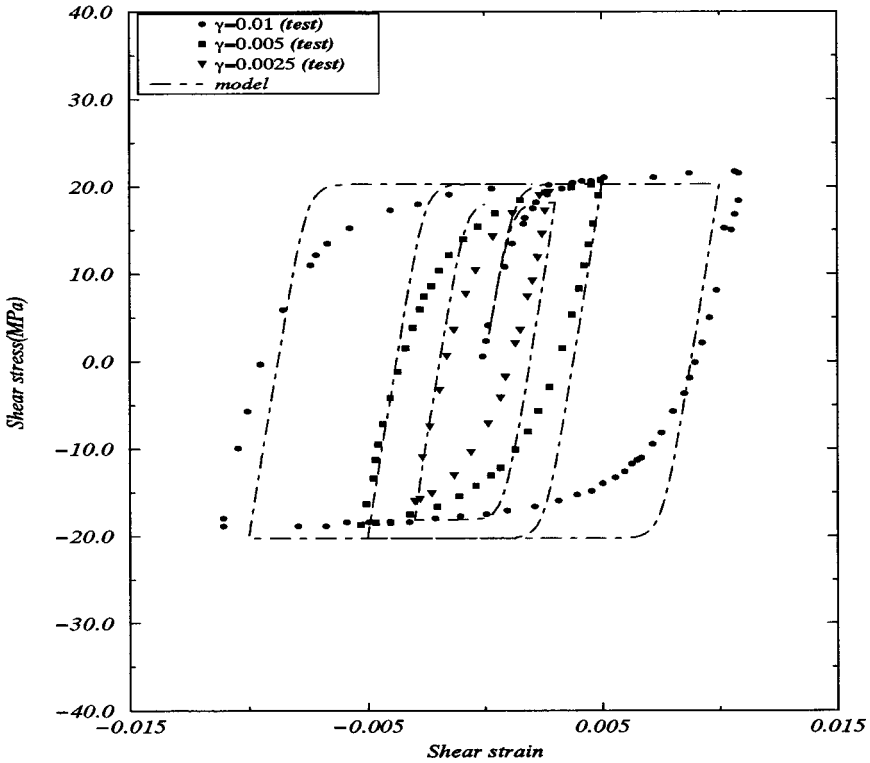

Fig. 4 Comparison of shear stress versus strain results at 22°C and strain rate of 0.003

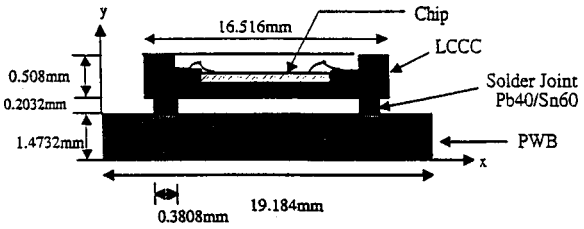

Fig. 5 A schematic of the SMT package

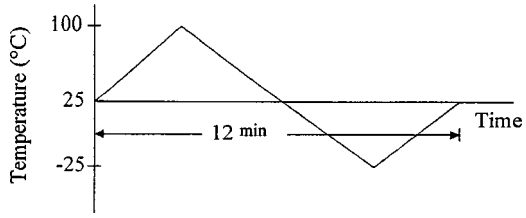

Fig. 6 Time history of thermal loading

$$d\varepsilon_{ij}^{\theta} = \alpha_T d\theta I_{ij} \tag{9}$$

where α_T is the coefficient of thermal expansion, $d\theta$ is the increment of temperature, and I_{ij} is the unit vector. The elastic strain increment is defined by,

$$d\varepsilon_{ij}^{e} = D_{ij}^{e} d\sigma_{ij} \tag{10}$$

Where D_{ij}^{e} is the inverse of the elastic constitutive tensor. In order to define the increment of the viscoplastic strain in Eq. (8) we need to define a viscoplastic strain rate function. Tin/Lead solder is a two phase alloy with an evolving microstructure. Chandaroy [13] has shown that the microstructure and grain size of a solder joint depends on its cooling rate, age, temperature and strain history. For Pb/Sn solder alloys, the creep function used must take into account the microstructure. Yet it should be simple enough to be used in a boundary value problem. For the constitutive model proposed in this paper the following strain rate function was adopted by Chandaroy [13],

$$\dot{\varepsilon}_{ij}^{vp} = A(\sinh[B\overline{\sigma}])^{n}(d)^{m} \exp\left[\frac{-Q}{k\theta}\right]\frac{\partial\overline{\sigma}}{\partial\sigma_{ij}} \tag{11}$$

where A, B, n, and m are material constants, $\overline{\sigma}$ is the von Mises equivalent stress and is given by $\overline{\sigma} = \sqrt{3J_{2D}}$, d is the average solder grain size, Q is the creep activation energy, k is the Boltzmann's constant, θ is the absolute temperature in Kelvin, and σ_{ij} is the total stress tensor. Visco plastic material properties are given in Table 1.

Verification of the Constitutive Model

To verify the constitutive model a series of laboratory test data was simulated. Adams [14] performed a series of tensile tests on Pb40/Sn60 bulk solder specimens, which were conducted on an Instron 1122. The tests were performed at constant temperatures between -55°C and 125°C over a range of strain rates from 8.33×10^{-5} to 8.33×10^{-2}. The tests were performed at constant crosshead speed, but since only small strain data was used this was assumed to be approximately constant true strain rate. The material parameters used are as follows: Young's modulus (E) and Poisson's ratio (ν) values were obtained by Adams from ultrasonic testing on bulk Pb40/Sn60 solder samples. The variation of E and ν

$$\mathrm{E(GPa)} = 62.0 - 0.067\,\mathrm{T} \quad \text{and} \quad \mathrm{G(GPa)} = 24.3 - 0.029\,\mathrm{T}$$

$$\upsilon = \frac{E}{2G} - 1$$

where G is the shear modulus and T is the temperature in Kelvin. Other material parameters used in the analysis are as follows;
Viscoplastic material parameters:

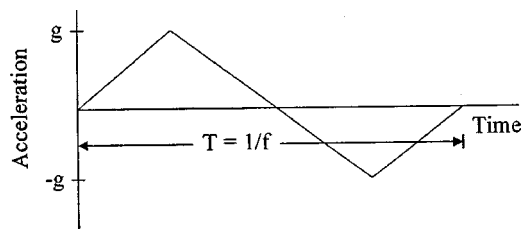

Fig. 7 Time history of dynamic loading

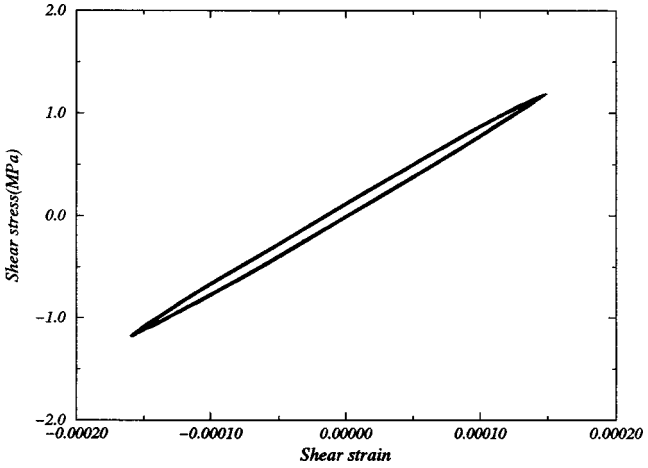

Fig. 8 Shear stress versus strain response for dynamic load of 5g–10Hz in both X and Y directions

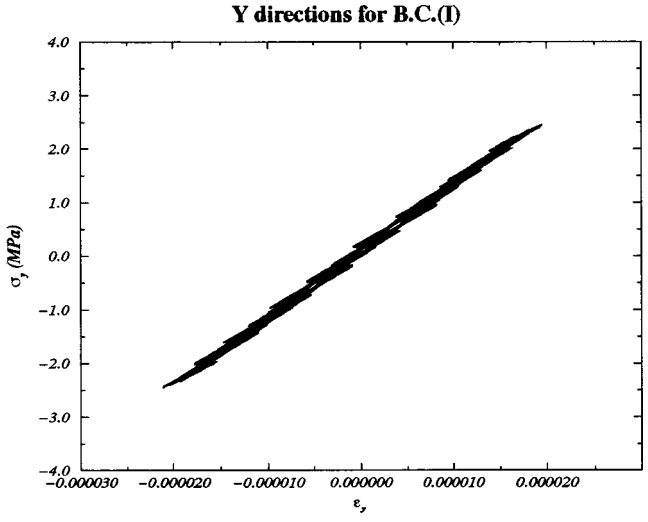

Fig. 9 Normal stress versus strain response for dynamic load of 5g–10Hz in both X and Y directions

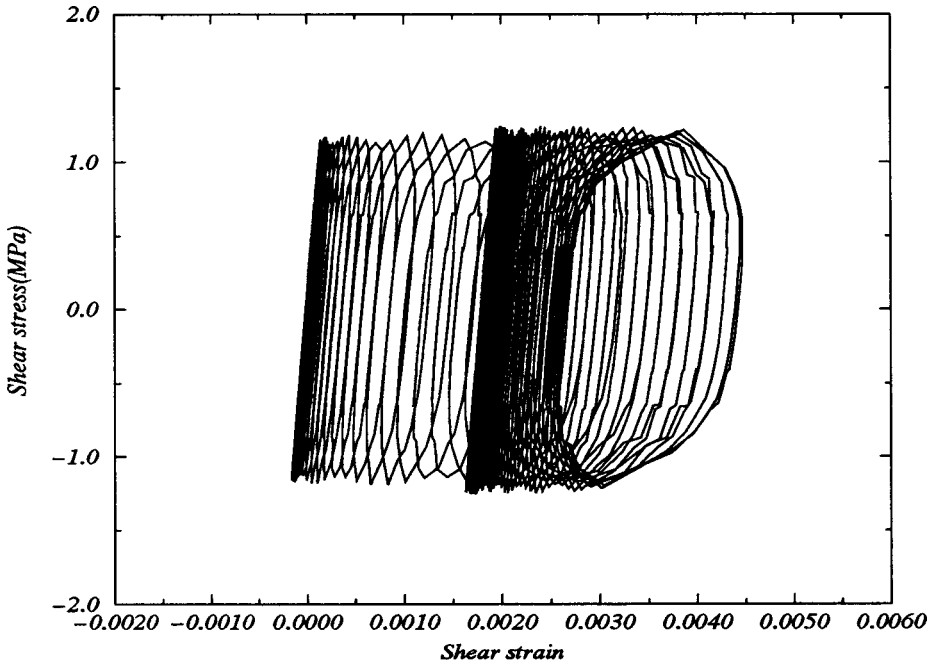

Fig. 10 Shear stress versus strain response for concurrent thermal and dynamic load 5g−10Hz in both X and Y directions

Table 1 Material parameters

Parameter	Value
A(s^{-1})	2.452×107
B	0.10726
N	2.4283
D	15 μm
M	−3.34
Q	57.3Kj/mole

For simplicity the von Mises yield surface with no hardening was used for strain rate function. Figures 1(*a*) and 1(*b*) show comparison between Adams test data and constitutive model simulations at different temperatures. The difference between simulations and test data at small strain levels could be due to the fact that hyperbolic sine creep models ignore primary creep. For practical engineering purposes simulations match test data well. Adding hardening function to yield surface would make the simu-

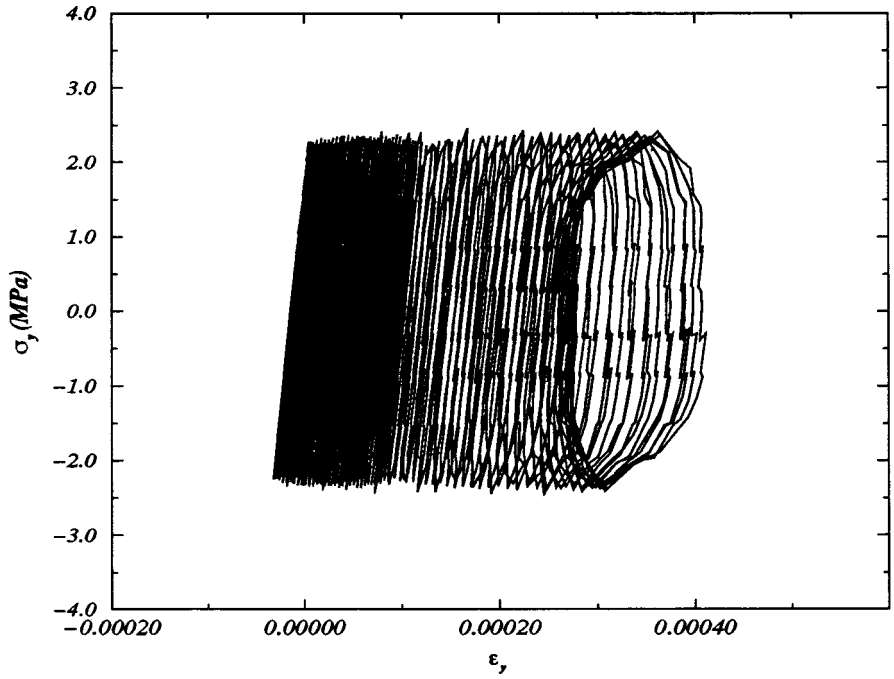

Fig. 11 Normal stress versus strain response for concurrent thermal and dynamic load 5g−10Hz in both X and Y directions

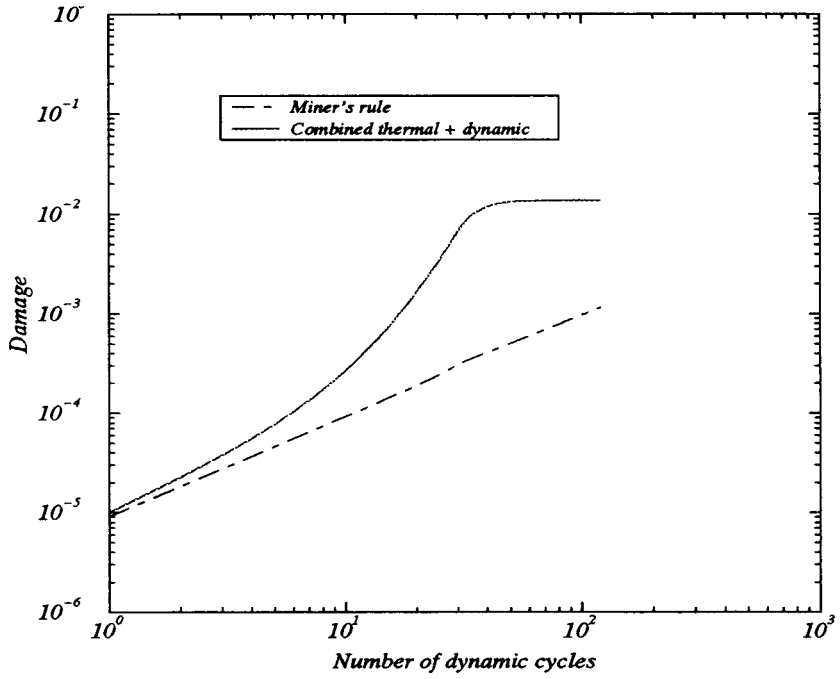

Fig. 12 Damage versus number of dynamic cycles for concurrent thermal and dynamic loading of 5g–10Hz in both X and Y directions

lation stress-strain curves smoother but would also increase the computation time.

McDowell et al., [15] performed tensile tests across a range of temperature and strain rates on a 62Sn-36Pb-2Ag solder alloy. Figures 2(*a*) and 2(*b*) show true stress-true strain response for different temperatures.

Busso et al., [16] performed cyclic shear tests on Pb40/Sn60 bulk solder that was casted in air into 30 mm diameter bars and subsequently machined into cylindrical specimens. The cyclic stress-strain behavior of the solder was determined from cyclic torsion tests performed on a feedback controlled servo-hydraulic testing machine. Cyclic tests were carried out under isothermal displacement controlled conditions with a ramp waveform and zero mean strain at a frequency of 0.01 Hz. The tests were controlled through the measured twist angle on the specimen's grip. Figure 3 shows the comparison between test data and constitutive model simulation.

Schroeder et al., [17] performed cyclic torsion shear tests under variable strain amplitudes on 63Sn-37 Pb eutectic solder alloy. Specimen blanks were cut to 2.5 cm by 2.5 cm by 17.8 cm and single point machined to 1.27 cm outside diameter over the gauge section. Specimens were then gun bored to inside diameter of 1.03 cm. All specimens were aged at 22C for over two months prior to testing to allow microstructural thermodynamic equilibration. Comparison between shear stress-shear strain test data and model simulations are given in Fig. 4 for different strain ranges.

Overall comparison of test data with constitutive model simulations agrees very well.

Analysis Of a Solder Joint Between a Ceramic Chip Carrier and a Printed Wiring Board

The fatigue life and stress-strain response of a Pb40/Sn60 solder joint in a surface mount technology package subjected to thermal cycling and vibrations are studied. The package shown in Fig. 5 was subjected to a temperature cycling and base acceleration. The time histories of the temperature cycling and the vibrations are given in Figs. 6 and 7, respectively.

Both low and high cycle fatigue were considered, since under dynamic loading, the behavior of the solder alloy can be elastic or inelastic depending on the acceleration and the frequency of the vibrations. For low cycle fatigue (up to 10^4 cycles Barker et al. [1]), the damage was calculated using Eq. (6). For high cycle fatigue (over 10^4 cycles, Barker et al. [1]), the damage was calculated using the following criterion, Barker et al. [1],

$$D = \Sigma (n_i / N_i) \tag{12}$$

where n_i is the number of cycles experienced and N_i is the total number of cycles to failure. High cycle fatigue life test data was obtained from the data presented by Steinberg [2].

The combined loading situation is first simulated by superposing the damage due to vibration and thermal loads using Miner's rule. The damage due to each loading type acting alone is determined and then superposed to assess the overall fatigue life of the joint, Barker et al., [1]. In the second stage, coupled thermo-viscoplastic-dynamic analyses are performed using the finite element procedure presented above, in which the total damage is computed directly.

In the literature and in the industry it is common practice to compute the total fatigue damage caused by vibration and thermal cycling using Miner's rule, Barker et al., [1].

A finite element analysis was conducted for the following load case. In the loading combination, the thermal cycling and the dynamic loading of 5 g-10 Hz are applied in both *X* and *Y* directions. Figures 8 and 9 show $\tau_{xy} - \gamma_{xy}$ response and the $\sigma_y - \varepsilon_y$ response, respectively, of the solder joint under dynamic loading only. Figure 8 shows that the maximum shear stress level is almost the same as when vibrations are applied in the *X*-direction only (not shown). This is in spite of the fact that, the energy dissipated in the joint is much larger due to the larger plastic strain. This is probably due to the contribution of the vertical displacements to the shear stress.

Figure 10 shows the $\tau_{xy} - \gamma_{xy}$ response in the solder joint under concurrent thermal and dynamic loading of 5 g-10 Hz in both *X* and *Y* directions. The maximum strain level reached is also larger when compared to thermal+single directional dynamic loading. As a result, having loading in both *X* and *Y* directions is the worst

combination. Another feature observed in this response is that with the reduction of temperature, the plastic strain starts to reduce but does not go to the original position at room temperature and even at lower temperatures, stops at a certain plastic strain level.

Figure 11 shows the $\sigma_y - \varepsilon_y$ response for the concurrent thermal and dynamic loading of 5 g-10 Hz in both *X* and *Y* directions. Comparing it with thermal plus single directional dynamic loading cases (where vibrations are applied only in *X* or *Y* directions), we can conclude that combining vibrations in *X* and *Y* directions does not make any difference in the $\sigma_y - \varepsilon_y$ response in the solder joint.

Figure 12 depicts the distribution of the coupled accumulative damage versus the number of dynamic cycles for the coupled analysis and for the analysis performed using Miner's rule. An order of magnitude difference is observed when coupled analysis results are compared with Miner's rule results. Miner's rule significantly underestimates the total damage, and as a result overestimates the fatigue life. The latter observation indicates that performing a coupled analysis is essential for any final analysis.

Since original submission of this paper we have done laboratory testing of solder joints under combined loading. Even though our test results do not exactly agree with results in this paper, test results strongly suggest that Miner's rule cannot be used for calculating combined environment damage values.

Conclusions

In this paper a unified constitutive model has been proposed for fatigue life predictions of solder joints in surface mount technology electronic packaging. Coupled thermo-viscoplastic-dynamic analysis results have been compared against fatigue life predictions using Miner's rule. The comparisons indicate that Miners rule significantly underestimates the accumulative damage in the system. The results indicate that the reliability of a solder joint cannot be solely determined by the thermal cycles experienced. It has been shown that dynamic loads can lead to low cycle fatigue without the existence of thermal loads. Obviously, the simultaneous application of thermal and dynamic loads significantly shorten the fatigue life.

In this study it has been shown that Miner's rule overestimates the fatigue life. Using Miner's rule for the preliminary analysis would be acceptable. But the final analysis should be performed for the coupled loading.

The results strongly suggest that having thermal loading in conjunction with dynamic loading makes a significant difference in the fatigue life of the solder joint.

Acknowledgments

The research results reported herein were supported by Grant No. N00014-97-1-0685 from the Department of Defense Office of Naval Research Young Investigator Award Program. The Program Director for the project is Dr. Roshdy Barsoum of ONR. We are grateful for his valuable comments.

References

[1] Barker, D., Vodzak, J., Dasgupta, A., and Pecht, M., 1990, "Combined Vibrational and Thermal Solder Joint Fatigue-A Generalized Strain Versus Life Approach," ASME J. Electron. Packag., **112**, pp. 129–134.

[2] Steinberg, D. S., 1988, *Vibration Analysis for Electronic Equipment*, Wiley, New York, NY. Kashyap, B. P., and Murty, G. S., 1981, "Experimental Constitutive Relations for the High Temperature Deformation of a Pb-Sn Eutectic Alloy," Mater. Sci. Eng., **50**, pp. 205–213.

[3] Desai, C., 1995 "Constitutive Modeling Using the Disturbed State Concept," Chapter 8 in *Continuum Models for Materials with Microstructure*, H. B. Muhlhaus, ed., Wiley, UK.

[4] Desai, C. S., and Toth, J., 1996, "Disturbed State Constitutive Modeling Based on Stress-Strain and Nondestructive Behavior," Int. J. Solids Struct., **33**, No. 11, pp. 1619–1650.

[5] Desai, C. S., Chia, J., Kundu, T., and Prince, J. L., 1997, "Thermomechanical Response of Materials and Interfaces in Electronic Packaging: Part I-Unified Constitutive Model and Calibration," J. Electron. Packg., **119**, No. 4, pp. 294–306.

[6] Basaran, C., Desai, C. S., and Kundu, T., 1998, "Thermomechanical Finite Element Analysis of Microelectronics Packaging, Part I: Theory," ASME J. of Electronic Packaging, **120**, No. 1, pp. 41–47.

[7] Basaran, C., Desai, C. S., and Kundu, T., 1998, "Thermomechanical Finite Element Analysis of Microelectronics Packaging, Part I: Verification and Application," ASME J. of Electronic Packaging, **120**, No. 1, pp. 48–54.

[8] Basaran, C., and Chandaroy, R., 1999, "Nonlinear Dynamic Analysis of Surface Mount Interconnects, Part I: Theory," ASME Journal of Electronic Packaging, **121**, Mar.

[9] Basaran, C., and Chandaroy, R., 1999, "Nonlinear Dynamic Analysis of Surface Mount Interconnects, Part II: Applications," ASME Journal of Electronic Packaging, **121**, Mar.

[10] Basaran, C., and Yan, C. Y., 1998, "A Thermodynamic Framework for Damage Mechanics of Pb/Sn Solder Joints," ASME J. Electron. Packag. **120**, pp. 379–384. Basaran, G., and Chandaroy, R., 1997, "Finite Element Simulation of the Temperature Cycling Tests," IEEE Trans. CPMT. Part A **20**, No. 4, pp. 530–536.

[11] Basaran, C., and Chandaroy, R., 1998, "Mechanics of Pb40/Sn60 Near-Eutectic Solder Alloys Subjected to Vibrations," Journal of Applied Mathematical Modeling **22**, pp. 601–627.

[12] Boltzamnn, L., 1898, *Lectures on Gas Theory*, U. of California Press, Trans. by S. Brush 1964.

[13] Halliday D., and Resnick, R., 1966, *Physics*, Wiley, New York, NY.

[14] Chandaroy, R. 1998, "Damage Mechanics of Microelectronic Packaging Under Combined Dynamic and Thermal Loading," Ph.D dissertation, SUNY at Buffalo.

[15] Adams, P. J., 1986 "Thermal fatigue of Solder Joints in Micro-Electronic Devices," MS thesis, Dept. of Mechanical Engineering, MIT.

[16] McDowell, D. L., Miller, M. P. and Brooks, D. C., 1994 *Fatigue Testing of Electronic Materials*, ASTM STP 1153, pp. 42–59.

[17] Busso, E. P., Kitano, M., and Kumazawa, T., 1992, "A Viscoplastic Constitutive Model for 60/40 Tin-Lead Solder used in IC package Joints," ASME J. Eng. Mater. Technol., **114**, pp. 331–337.